Chinese Chemical Letters 36 (2025) 109941

Contents lists available at ScienceDirect

Chinese Chemical Letters

journal homepage: www.elsevier.com/locate/cclet

New insight into manganese-enhanced abiotic degradation of microplastics: Processes and mechanisms

Yunlong Sun[a], Wei Ding[a], Yanhao Wang[b], Zhening Zhang[a], Ruyun Wang[a], Yinghui Guo[a], Zhiyuan Gao[c], Haiyan Du[a], Dong Ma[a,*]

[a] College of Resource and Environment, Qingdao Agricultural University, Qingdao 266109, China
[b] School of Environmental Science and Engineering, Qingdao University, Qingdao 266071, China
[c] Bathurst Advanced Agricultural Technology Institute, Qingdao Agricultural University, Qingdao 266109, China

ARTICLE INFO

Article history:
Received 28 November 2023
Revised 28 March 2024
Accepted 28 April 2024
Available online 29 April 2024

Keywords:
Polyethylene
Microplastics
Manganese
Degradation
Carbonyl index

ABSTRACT

Microplastics (MPs) are an emerging environmental pollutant and have penetrated the most remote and primitive areas. MPs degradation has received widespread attention. Manganese (Mn) is a highly reactive metal element in the environment, yet its contribution to MPs degradation remains unclear. Herein, we simulated the aging of polyethylene MPs with Mn(II) under aqueous conditions at pH 5 and 8 for 720 days. Mn greatly promoted the MPs degradation, and the average particle sizes of polyethylene MPs were reduced from 9.2 μm to 5.9 μm after aging at pH 5 under light irradiation for 720 days. Plenty of oxygen-containing groups were generated on the MPs surfaces, and the carbonyl index remarkably increased, reaching four times that of the control without adding Mn. Mechanistically, the adsorbed Mn(II) on the MPs surfaces were primarily oxidized to high-valence Mn(III/IV) profited from the photoproduced radicals, followed by the MPs oxidation *via* Mn(III/IV), which were reduced to regenerate Mn(II), initiating a new redox cycling. During the degradation, dissolved organic matter was continuously released, mainly including bisphenol A and phthalic acid esters. Mn acts as a catalyst to accelerate the MPs degradation by redox cycling. Our results provide a new insight into the mechanisms of abiotic degradation of MPs in aqueous environments.

Microplastics (MPs) are emerging environmental pollutants that are difficult to degrade naturally due to their stable chemical properties and exist in the environment for a long time [1,2]. Previous works show that plastics have infiltrated some of the planet's most remote and pristine areas, emphasizing the urgent need to reduce their impact [3,4]. MPs are acknowledged to promote the diffusion and ecological implications of pollutants, and the understanding of their involvement in these processes has received increasing scholarly attention [5,6]. Notably, approximately 85% of MPs enter water, and aquatic circumstances become the largest storage repository of these substances [3,7]. In aquatic circumstances, a potential interaction exists between quantitative manganese (Mn) in water and MPs. However, research on the impact of Mn on MP aging is still limited, especially that of aquatic Mn(II). Classifying this process is crucial to understand their long-term behavior and ecological impact.

MPs are broadly defined as plastic fragments with a particle size of less than 5 mm. They are difficult to decompose in the natural environment completely. However, partial aging occurs under many conditions, and this process is a synergy of physical and chemical changes [8,9]. Weather, water erosion, mechanical wear, and human activities further reduce the size of MPs, and smaller sizes are conducive to better diffusion of MPs in the environment [10,11]. For example, MPs with particle sizes less than 50 μm in atmospheric MPs accounted for 70%–80% of the total MP deposition in the North China Plain [12]. In shallow water environments, there are large amounts of suspended MPs [7]. After photoaging, chemical oxidation, and biological action, the density and chemical properties of MPs are changed [10,13,14]. The aging process alters the hydrophobic structure of the MP polymers, and the formation of oxygen-containing groups improves the hydrophilicity of MPs, promoting their vertical distribution in the aqueous environment [8,15]. In industrial production, chemical additives, such as plasticizers and antioxidants, are commonly added during plastic processing to enhance material properties. These substances are typically connected to polymers through hydrogen bonds, making them susceptible to environmental exposure [16,17]. Long-term contact of plastics with water significantly increases the risk of dissolving additives. During plastic aging, the continuous crushing ex-

* Corresponding author.
E-mail address: dma796@hotmail.com (D. Ma).

https://doi.org/10.1016/j.cclet.2024.109941
1001-8417/

pands the specific surface area of plastics, promoting the release of dissolved organic matter (DOM). During MP aging, the long carbon chain breaks to form small molecules of organic substances, such as organic acids, alcohols, and aldehydes [13]. These products change the pH and electronegativity of the microenvironment surrounding the MPs and can be used as nutrient sources for environmental microorganisms [1]. Aging MPs have a strong adsorption capacity for organic pollutants, increasing the risk of biological ingestion, and the combined toxicity of this mixture is also a concern [18,19]. MPs can also adsorb heavy metal elements in the environment, and this adsorption capacity can be greatly enhanced by the oxygen-containing groups on the surface of aging MPs [20]. The reported results of the adsorption test of Mn(II) by naturally- and artificially-aged MPs showed that the adsorption capacity of aging MPs to Mn(II) was substantially improved due to the increasing oxygen-containing groups and specific surface area [21]. Moreover, the mechanism by which the adsorbed Mn(II) affects the MP aging is worth further exploration to reveal the redox cycling of the adsorbed Mn(II) and MPs.

Mn is a widely distributed and chemically active metal element in the geosphere and is important in geochemical processes [22]. Mn(II) is ubiquitous in the photic zone of surface waters, usually in $MnCl^+$ ligands and complexes combined with small organic matter [23]. In addition, it can be oxidized by chemical and biological procedures to form Mn hydroxides and granular Mn oxides (MnO_x) in aqueous environments [23,24]. The high-valence Mn (hydro)oxides possess high oxidizing properties in the natural environment, and the enhanced degradation and mineralization of natural organic matter are attributed to the oxidization by electron transfer or reactive oxygen species [16,22]. Despite the reported degradation of organic pollutants by Mn (hydro)oxides, MPs decomposition has rarely been mentioned. As an artificial organic matter, MPs can be affected during aging.

The present work investigates the chemical interaction between Mn and MPs during MPs aging in Mn-rich environments. Polyethylene (PE) is a commonly used plastic material among polymers. It is widely processed into agricultural mulch film, plastic wrap, plastic bags, and other packaging products [9]. In this study, PE was selected as a representative of MPs. The influence of environmental factors on the aging process was also investigated by controlling the light conditions and initial pH during reactions (see details in the Experimental Section in Supporting information). Despite the deep understanding of the Mn(II) absorption by MPs, the role of MPs aging-induced small molecules is overlooked. These products are retained in the system and participate in subsequent aging reactions.

PE is a highly hydrophobic and non-polar polymer with a density lower than that of water. During various aging treatments, PE particles floated on the liquid surface, forming a distinct interface with an aqueous phase. With progressive aging, the interface between the aged PE and the aqueous phase began to diffuse, indicating a change in the hydrophobicity of the aged PE [11]. The contact angle of the original PE particles is ~109.4°, as shown in Fig. 1. After 720-day (720-d) aging, these particles are suspended in an aqueous phase and re-layered within a few minutes. The contact angle of the aged PE particles was pronouncedly decreased to 77.7° with the presence of Mn(II) and natural light exposure at pH 5. The contact angles of aged PE particles with Mn(II) and light were 93.6° and 101.8°, respectively, indicating that both treatments contribute to the hydrophilic tendencies in the aged PE.

Scanning electron microscope (SEM) was performed to observe the morphology of the aged PE particles. Original PE particles exhibit irregularly shaped granular or long strips, with an average particle size of about 9.2 μm (Fig. 2, Fig. S1 and Table S1 in Supporting information). By zooming in, uneven folds are discovered on the surfaces of the PE particles. The particle sizes of the aged PE

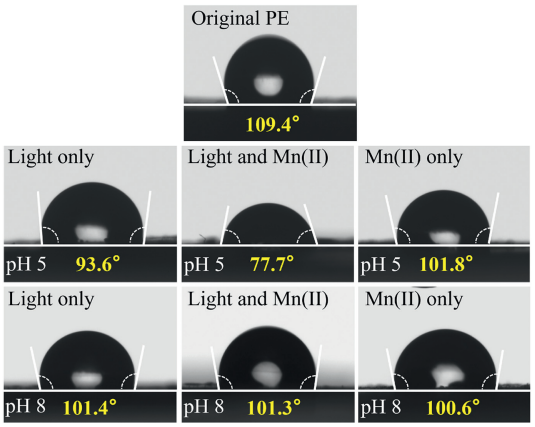

Fig. 1. Contact angles of original PE and PE after different aging treatments.

samples are noticeably decreased under Mn(II) addition and natural light exposure at pH 5. The decrease of the particle size was changed gradually according to the aging time, and the average particle size of the aged PE after 720 days was about 5.9 μm (Figs. 2a–e). The aged PE particle surfaces exhibit holes and cracks not found in the treatment without light irradiation (Fig. S2c in Supporting information), suggesting that light is the primary driving factor for PE aging. In contrast, only cracks are found on the PE particle surfaces without the addition of Mn(II) (Fig. S2a in Supporting information), demonstrating that Mn(II) accelerates the PE aging and fragmentation under these light-induced processes. The surface of the original PE exhibits substantial carbon elements and a scarcity of oxygen elements, implying that only a small portion of the PE surface undergoes oxidation (Fig. 2a1). Following aging with Mn(II) addition and natural light exposure at pH 5 for 720 days, oxygen elements on the surface of the PE are enriched, accompanied by a significantly higher content of Mn(II) than its surroundings (Fig. 2e1). This suggests that the adsorption capacity of the aged PE for Mn is increased, consistent with previous research findings [13,21]. It was inferred that the PE aging first contributed to the deepening of folds and formation of cracks on the surfaces under the light irradiation, followed by the formation of deep cracks and holes after adding Mn(II) [13,20]. The combined action of Mn(II) and light irradiation can be the key cause of the accelerated decrease in PE particle size.

PE MPs are composed of a hydrocarbon structure and are unfavorable to oxidizing to oxygen-containing groups on the surfaces [10,25]. Herein, Attenuated total reflectance - Fourier transform infrared (ATR-FTIR) spectroscopy was employed to identify the surface chemical structure of PE particles. Five main peaks are identified in the FTIR spectra of the original PE particles (Figs. 3a-c). The peaks attributed to the asymmetrical and symmetrical telescopic vibrations of $-CH_2$ groups are at 2916 and 2848 cm^{-1}, respectively. The peak at 1471 cm^{-1} is assigned to the antisymmetric bending vibration of $-CH_3$ groups. The peaks at 1462 cm^{-1} and 720 cm^{-1} correspond to the bending and rocking vibration of $-CH_2$ groups [25]. The Raman spectra of PE particles show consistent results (Fig. S3 in Supporting information). No signals of oxygen-containing groups (*e.g.*, carbonyl and hydroxyl) are detected in the original PE particle surfaces. As shown in Fig. 3b, a telescopic vibration peak of C=O appears at 1712 cm^{-1} in the spectra of aging PE particles with Mn(II) addition and natural light exposure at pH 5, suggesting the occurrence of physical or chemical aging of PE [27]. The addition of Mn(II) substantially enhances the formation of the oxygen-containing groups according to the intensities of the vibration peaks of carbonyl groups (Figs. 3b and c). By contrast, light irradiation exhibits insufficient oxidative activity for increased for-

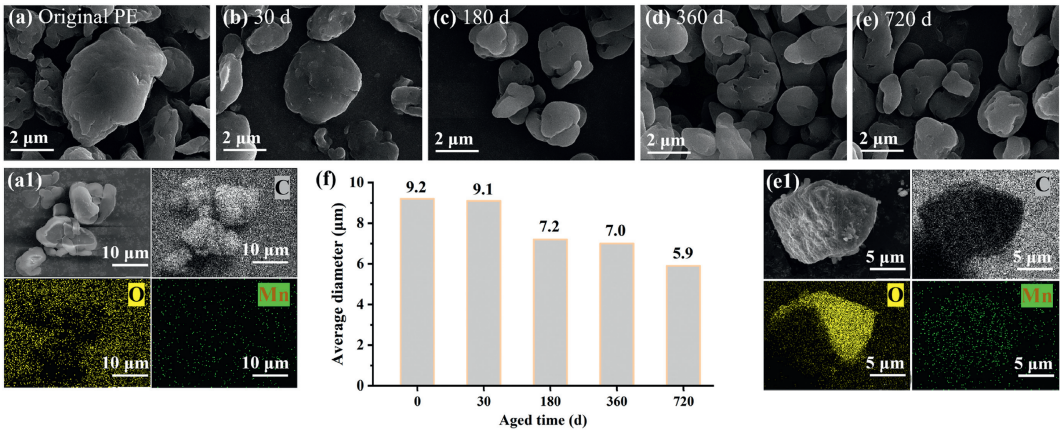

Fig. 2. SEM images of original PE particles (a) and the PE particles after aging with the presence of Mn(II) and natural light exposure at pH 5 (b–e). Elemental mapping images of original PE particles (a1) and the PE particles after 720 d of aging (e1). Histogram of particle size (diameter) of original and aged PE particles (f).

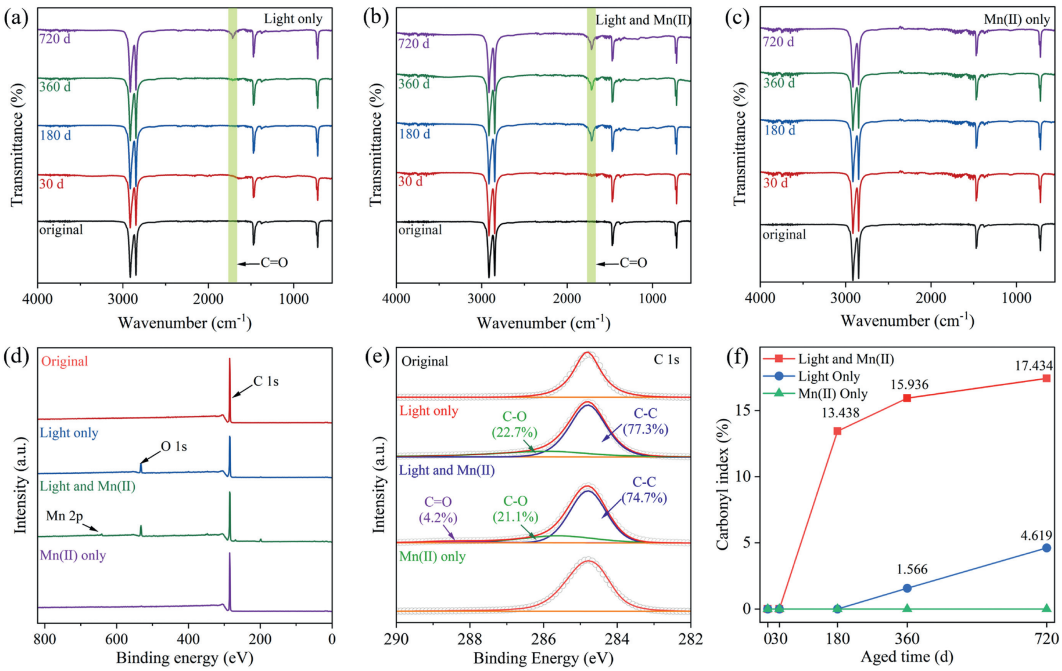

Fig. 3. ATR-FTIR set of spectra for PE particles after different aging treatment (a–c). XPS survey (d), the high-resolution XPS spectra of C 1s (e) on original and aging PE particles. The trends in the CI of different treatment (f). All reactions were conducted at pH 5.

mation of carbonyl groups, and the presence of Mn(II) accelerates the production of carbonyl groups on the aging PE surfaces under light irradiation, remarkably promoting the degradation of PE. The consistent results were verified from the X-ray photoelectron spectroscopy (XPS) spectra of the aged PE particles. The XPS spectra of the original PE demonstrate that only one spin-orbit peak of C 1s appears at binding energies of 284.8 eV, representing the C–C structure in PE surfaces [28], as shown in Fig. 3d. The O and Mn elements are detected in the aged PE samples, and high-resolution XPS spectra of PE samples show two and three distinct spin-orbit peaks, respectively. The potential reason for this is that the PE produces oxygen-containing groups during aging under light irradiation (Fig. 3e). The addition of Mn(II) boosts carbonyl groups after adding Mn(II) under irradiation, due to the synergistic effect of both actions [28,29]. The controlled trials result further verified that Mn(II) alone can hardly afford the production of carbonyl groups on PE surfaces.

The carbonyl index (CI) is widely deployed to evaluate the degree of polymer oxidation, enabling quantifying some changes in the material chemical structure. The ATR-FTIR spectra obtained from PE with different aging treatments were used to calculate the CI [26,27]. The aging kinetics of PE with different treatments were quantified by comparing the CI, as illustrated in Text S1 (Supporting information). At pH 5, the changing trend of CI of PE MPs with different treatments is shown in Fig. 3f. Carbonyl peaks are detected in PE MPs under natural light and 360-day aging. In the case of 720-day aging, the CI reaches a maximum of 4.6%. Carbonyl formation was detected after aging with the Mn(II) addition and natural light exposure at pH 5 for 30 days. The CI increases rapidly to 11.4% within 180-day aging and slowly increases to 17.4% during the remaining aging period, which reaches four times that of the control group. The possible reason for these phenomena is that the intensity of the symmetrical telescopic vibration peak of $-CH_2$ decreases with progressive oxidation. In this process, the long-carbon chains of PE fracture, and fragmentation occurs in the PE particles. Due to the hydrophilic nature of the carbonyl groups, these two naturally photoaging-treated samples are dissolved, consistent with the result in the water contact angle test of the samples.

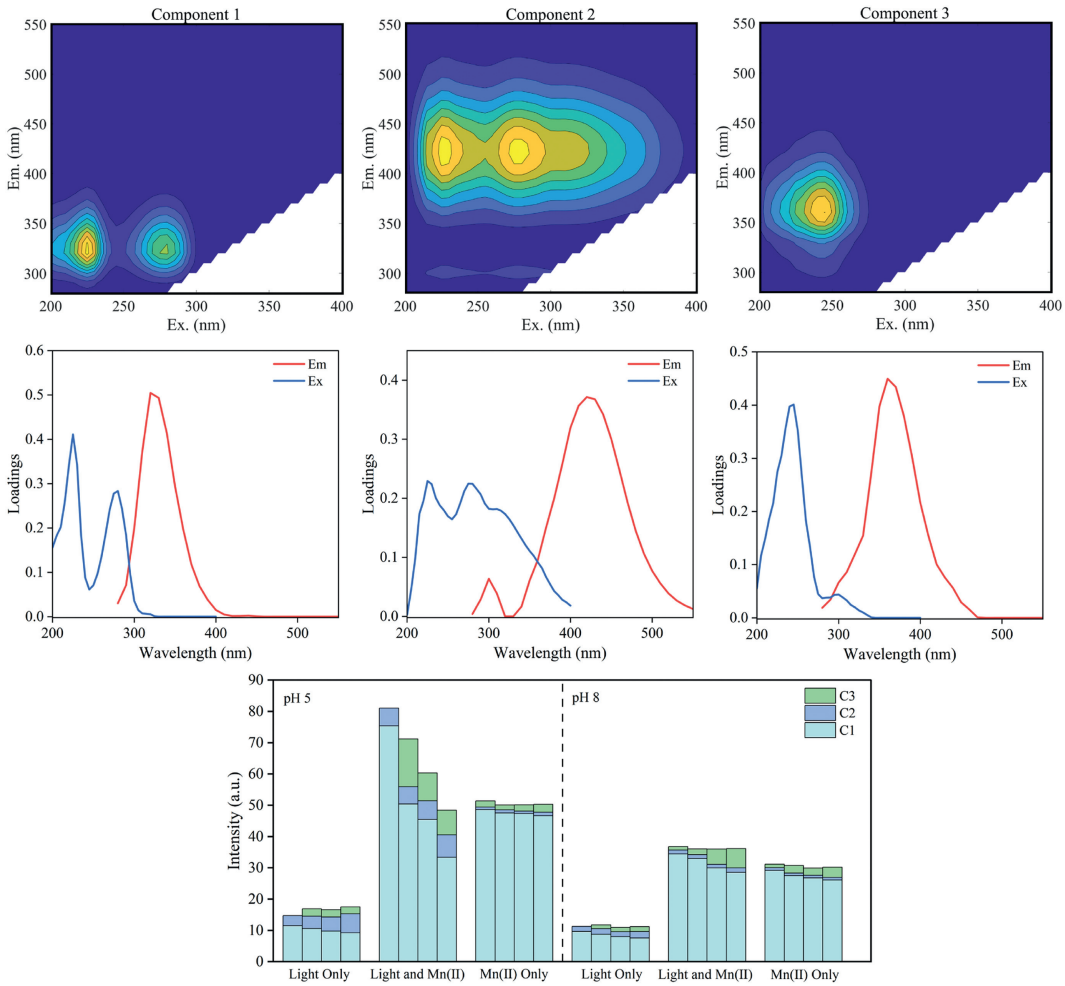

Fig. 4. Spectral characteristics of the three components (C1-3) PARAFAC modeling of PE MPs dissolved products. Histogram of DOM content at different treatment dissolved products and different reaction stages was analyzed by EEM-PARAFAC. In each set of histograms, four columns stand for 30 d, 180 d, 360 d, and 720 d from left to right, respectively.

The changes in the crystalline structure of original and aged PE MPs were analyzed using XRD technology [30]. Three main crystal peaks are observed in the XRD patterns of PE at 19.9°, 21.5°, and 23.9° (Fig. S4a in Supporting information) [10]. To understand the variations in the crystal structure of MPs in different sets, the crystallinity of each sample was calculated, and the detailed method is described in Text S2 (Supporting information). Crystallinity trends of samples with various aging treatments are shown in Fig. S4b (Supporting information). The initial crystallinity of the original PE is 32.94%, and the crystallinity of aging PE particles under light irradiation at pH 5 slowly increases to 36.76%, indicating that the amorphous region of PE MPs is more likely to be oxidized and decomposed than the crystalline part. With the completion of aging, the oxidation of branched chains enhances the symmetry of PE molecules, and various oxygen-containing groups produced during the aging strengthen the hydrogen bonds between PE molecules, improving their crystallinity [31,32]. With the increasing crystallinity of PE molecules, the polymer becomes increasingly susceptible to fracture, accounting for the presence of small PE particle fragments in SEM images. Without light irradiation or Mn(II), the crystallinity decreases to varying degrees due to the changed crystalline region inside the polymer to an amorphous region under light conditions [33]. In addition, the disordered movement of water molecules weakens the crystallinity of the PE MPs [31,34].

The three-dimensional fluorescence spectrum is extensively applied for analyzing DOM composition [35,36]. The location, contour, and spectral loading of the Fluorescence excitation-emission matrix (EEMs) are shown in Fig. 4. Three distinct components are C1 (225 nm/280 nm, 320 nm), C2 (225 nm/280 nm, 420 nm), and C3 (245 nm, 360 nm). Based on the comparison of the database information with the current results, the C1 component is identified as a dissolved derivative of bisphenol A (BPA), C2 is from a phthalate ester, and C3 is an oxidation product of BPA [37]. Fig. 4 presents a stacked column chart of the content of different fluorescent products in liquid samples. A marked difference is detectable in the fluorescent content between the control group exposed to natural light and the control group containing Mn, probably due to the relatively high ionic intensity of the solution. Light exposure promotes the separation of these components, aligning with previous research findings [38]. In the early stages of aging, the PE MPs produce the largest number of fluorescent substances after adding Mn(II) and exposing them to natural light at pH 5. This is attributed to the altered surface morphology of PE MPs, reducing the particle size and the generation of fractures on the surface. In addition, various additives within the MPs particles are released into the aquatic environment [39]. With progressive aging, the content of C1 components in the produced fluorescent substances decreases owing to the oxidation of BPA, increasing the content of C3 components, and then the C3 was further oxidized

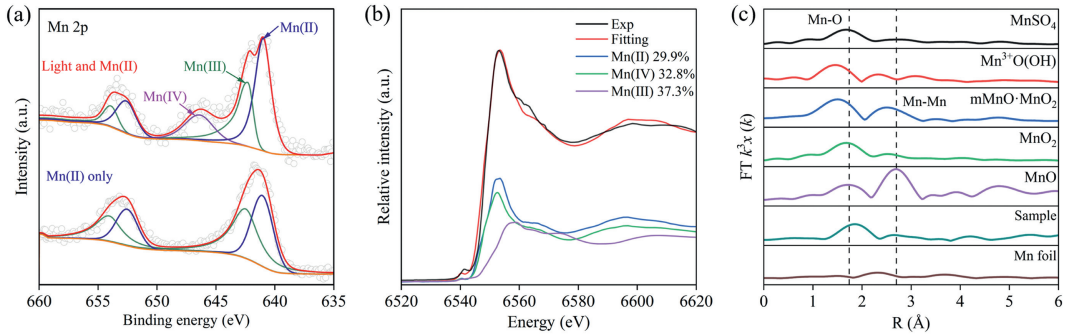

Fig. 5. (a) XPS spectra of Mn 2p on original and aging PE particles. (b) Normalized Mn edge XANES spectra of PE particles aging with the presence of Mn(II) and natural light exposure at pH 5. (c) Mn K-edge FT-EXAFS spectra for aging PE particles.

to a non-fluorescent product. Therefore, the C1 and C3 components in the system showed a trend of first increasing and then decreasing. During this period, the content of the C2 components remains stable and is the highest of all control groups, arising from the strong oxidation resistance of phthalates. The lowering content of fluorescent components is also attributed to the expanding specific surface area of aging PE MPs and the increasing adsorption capacity of organic substances, dynamically transforming the adsorption balance of organic matter on the surface of MPs [21]. In the control treatment, with the absence of Mn(II) and light, the DOM concentration of the solution remains relatively stable. In the early reaction stages, the main fluorescent components in the solution include C1 and C2. With further aging, a small number of C3 components are generated.

The total organic carbon (TOC) content of PE solutions under various aging treatments was tested to understand the variation in the content of non-fluorescent DOM (Fig. S5 in Supporting information). In the control group protected from light, TOC remains below the detection threshold of an instrument, illustrating that light is necessary for PE dissolution. Under natural light, the addition of Mn(II) in the solution remarkably increases the TOC. During the synergistic treatment of light and Mn(II), the increasing TOC in solution indicates a trend of first slow and then fast speed, and the reason for this is that aging MPs exhibit a relatively large irradiated area. The role of Mn(II) in this reaction needs to be further explored.

Compared with the control group exposed to natural light, the physicochemical properties of PE change dramatically after adding Mn(II) at pH 5. By contrast, Mn(II) rarely promotes PE aging in the control group without light treatment. For this reason, further analysis of the transformation of Mn species is needed. The high-resolution XPS spectra of the PE with different aging treatments Mn 2p are shown in Fig. 5a. The characteristic peaks at 640.9 and 652.6 eV were attributed to Mn(II), and those at 642.3 and 653.9 eV were allocated to Mn(III). The peak at 646.4 eV corresponding to Mn(IV) was detected only under irradiated conditions [40], indicating the formation of high-valance Mn species on the surface of PE MPs. In addition, the strong redox ability of these species greatly promotes the aging of PE MPs.

To further analyze the chemical composition of the generated high-valence Mn species at an atomic level, the Mn–K X-ray absorption near-edge structure (XANES) and Extended X-ray absorption fine structure (EXAFS) of the sample were collected [41]. The fitting results of the normalized Mn K–edge XANES spectra (Fig. 5b) show that the reaction-induced MnO_x was a mixture of MnO_x in different valence states, including 37.3% Mn(II), 29.9% Mn(III) and 32.8% Mn(IV), and the average oxidation valence state of Mn was 2.96 [42,43]. The high-valance Mn in MnO_x is the main part of electron transfer and loses electrons during the reaction. The presence of the low-valence Mn promotes the surface defects of MnO_x, enhances the adsorption capacity of its surface for oxygen, and promotes the process of electron transfer [16,43]. These results exhibit good agreement with those of XPS, proving that the Mn adsorbed on the surface of aging PE MPs undergoes a valence cycle, promoting the aging of MPs. Fig. 5c is the Mn K–edge EXAFS $k^3\chi$ (k) curves for the samples and standard ones. For the surface structure of these samples, the Fourier transform peaks assigned to Mn–O bonds, which represents the coordination of Mn with the adjacent oxygen atoms in the octahedral units of [MnO_6], is observed at 1.89 Å, and the Mn connected by oxygen atoms between adjacent [MnO_6] units is observed at 2.89 Å [44,45]. This finding indicates that the generated MnO_x is a mixed structure of MnO_2 and Mn_2O_3, and partial free Mn(II) adsorbed between molecules is observed.

Three control tests at pH 8 were set up to further explore the PE aging process in the natural environment, and the rest of the reaction conditions were consistent with the above tests except for the initial pH value. No significant difference in contact angle is observed in the aged PE (Fig. 1), and the decrease in contact angle is attributed to the long-term wetting of the aqueous solution. Furthermore, discoloration is presented in the PE particles due to the formation of brown precipitates by Mn(II) under pH 8. The PE surface of samples treated under alkaline conditions boosts folds, and the particle size of the PE MPs was consistent with the original one (Fig. S2). Nanoscale MnO_x clusters are detectable on the surface of the PE samples aging with Mn(II) at pH 8. Compared with the reaction under pH 5, no significant carbonyl formation is observed during the PE aging under pH 8 (Fig. S6 in Supporting information). The infrared absorption characteristic peak of MnO_x appeared in the range of 400–700 cm^{-1} [16]. However, no crystalline peak of MnO_x was seen in the XRD diffraction pattern, suggesting that the produced MnO_x was masked due to the low amount. The DOM species and concentrations at pH 8 were consistent with those at pH 5. An increasing C3 component is detected in the liquid sample at pH 8 when the reaction progresses. This is attributed to the facile oxidation reaction of BPA, which can react with OH^- in the solution to generate intermediate products more susceptible to oxidation than BPA [46]. Compared with the treatment at pH 5, the photoaging process of PE is inhibited at pH 8, and nanoMnO_x particles slightly promote the aging of PE MPs.

Herein, we conclude the effects of pH on MPs aging with Mn(II). Firstly, photogenerated free radicals have been recorded as the major driver for MPS aging without Mn(II) [13]. At low pH conditions (pH 5), more free radicals were generated by light irradiation, and MPs were continuously aged. High pH conditions mean more OH^- in the solution, and more free radicals would be captured by OH^-, significantly inhibiting the MPs aging. Secondly, low pH favors high catalytic contributions of Mn(II). As we know, Mn(II) is

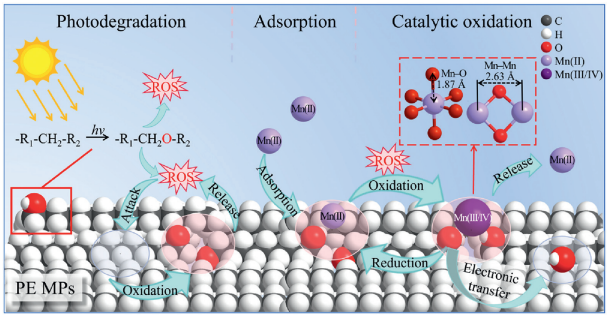

Fig. 6. Possible degradation mechanisms of PE MPs with the presence of Mn.

stably at low pH conditions, and the plenty of Mn(II) ions would be adsorbed and evenly distributed on the MPs surfaces [47]. The Mn(II) could act as an electron transmitter to accelerate the MPs aging. At high pH conditions, however, the Mn(II) would be easily oxidized into Mn oxides and become a protective layer on MPs surfaces, even though there are fewer radicals left. Thus, it indicates that low pH favors MPs aging, and Mn(II) accelerates MPs aging as an electron transmitter at low pH conditions.

The possible degradation mechanisms of PE MPs with the presence of Mn are concluded according to Fig. 6. Photodegradation is an important non-biological means of MPs decomposition from the environment [8,11]. In this process, PE molecules absorb light energy at specific wavelengths, breaking C–H bonds and forming free radicals, which usually occur in the side chains of PE [13]. A portion of the generated free radicals are released into the aqueous environment and combine with oxygen to form various small molecule inert products [14]; The rest remains on the surface of the PE MPs, which promotes the formation of oxidation defects on the PE surface. The presence of these oxidation defects significantly enhances the adsorption of the PE to free Mn(II) in solution [21,47]. By comparing the XPS results of aged PE subjected to different treatments, it is suggested that Mn(II) adsorbed on the PE is transformed into highly oxidized Mn(IV) species under light irradiation at pH 5. These high-valence Mn oxides are also products of free radical oxidation [24]. The generated Mn(IV) further oxidized PE MPs through electron transfer and Mn(IV) reduction [48,49]. Combined with the changes in the Mn(II) concentration in the solution (Fig. S7 in Supporting information), the adsorption of Mn(II) on the MPs surface promoted the generation of high-valance Mn species, which then increased the concentration of organic components in the solution, further promoting the adsorption of free Mn(II) [50]. Due to the cooccurrence of free radical reactions and electron transfer pathways of high-valence Mn, Mn-containing systems presented a more significant effect on the aging of PE MPs than the pure water systems, consistent with the reported results [17,51]. The amorphous regions of PE MPs were prone to oxidation, increasing the crystallinity of PE particles and their breaking tendency [52]. During the aging process, the particle size of PE MPs significantly decreased, and the surface became rougher with more pores.

By simulating the aging process of PE MPs with the addition of Mn, the morphology, chemical structure, and crystallinity of the PE MPs were analyzed over a long period. With the absence of Mn(II), PE MPs were partially oxidized due to the presence of proton in water, and a small quantity of C–O bonds were observed in PE MPs surfaces under light irradiation at pH 5. By contrast, PE MPs at pH 8 have slight oxidation, which is attributed to the photo-generated radicals under light irradiation. With Mn(II) presence, pronouncedly high surface oxidation of PE MPs was detected at pH 5. This result probably arose from Mn(IV) generation, verified by XPS and XAFS spectra. Mn(IV) plays a key role in accelerating the PE MPs aging, and the steps attributed to this phenomenon are summarized as follows: (i) Photo-generated radicals produce Mn(II) adsorption on PE MPs surfaces at oxidized sites; (ii) Mn(IV) is formed due to Mn(II) oxidation by some radicals; (iii) surficial decomposition of PE MPs is accelerated by Mn(IV) due to the electron transport; (iv) the accumulation of Mn(II) adsorption and Mn(IV) reduction form a redox cycling to sustain the surficial decomposition of PE MPs. With the increasing oxidization groups and CI values, the diameter of the PE MPs continued to decrease from 9.2 μm to 5.9 μm throughout the aging for 720 days. In addition to surficial decomposition, some hazardous DOMs, such as BPA and phthalate esters, were found to be released into water environments. The findings in this work are insightful for the mechanisms of abiotic degradation of MPs in aqueous environments, providing a novel strategy for artificial depolymerization of MPs pollutants by the Mn-based oxidation technique.

Declaration of competing interest

We declare that we have no financial and personal relationships with other people or organizations that can inappropriately influence our work, there is no professional or other personal interest of any nature or kind in any product, service and/or company that could be construed as influencing the position presented in, or the review of, the manuscript entitled.

CRediT authorship contribution statement

Yunlong Sun: Conceptualization, Data curation, Software, Writing – original draft, Formal analysis. **Wei Ding:** Data curation. **Yanhao Wang:** Data curation, Investigation, Project administration. **Zhening Zhang:** Data curation. **Ruyun Wang:** Data curation, Software. **Yinghui Guo:** Data curation, Formal analysis, Software. **Zhiyuan Gao:** Data curation. **Haiyan Du:** Software. **Dong Ma:** Funding acquisition, Investigation, Project administration, Supervision, Writing – review & editing, Resources.

Acknowledgments

This work was supported by the National Natural Science Foundation of China (No. 42077120), the Special Foundation for Taishan Scholar of Shandong Province (2023), and the Project of Talent Introduction and Education Program of Youth Innovation Teams in Universities of Shandong Province (No. 2021-05).

Supplementary materials

Supplementary material associated with this article can be found, in the online version, at doi:10.1016/j.cclet.2024.109941.

References

[1] F. Zha, M. Shang, Z. Ouyang, X. Guo, Gondwana Res. 108 (2022) 60–71.
[2] W. Tian, P. Song, H. Zhang, et al., Prog. Mater. Sci. 132 (2023) 101035.
[3] J. Gong, P. Xie, Chemosphere 254 (2020) 126790.
[4] J. Zhang, S. Ren, W. Xu, et al., J. Hazard. Mater. 435 (2022) 129065.
[5] S. Abbasi, F. Moore, B. Keshavarzi, et al., Sci. Total Environ. 744 (2020) 140984.
[6] P. Kang, Y. Zhao, C. Zuo, et al., Sci. Total Environ. 878 (2023) 163028.
[7] F. Dubaish, G. Liebezeit, Water Air Soil Pollut. 224 (2013) 1352–1360.
[8] W. Hamd, E.A. Daher, T.S. Tofa, J. Dutta, Front. Mar. Sci. 9 (2022) 885614.
[9] A.L. Andrady, Mar. Pollut. Bull. 119 (2017) 12–22.
[10] M.N. Miranda, M.J. Sampaio, P.B. Tavares, A.M.T. Silva, M.F.M. Pereira, Sci. Total Environ. 796 (2021) 148914.
[11] Y. Sun, J. Yuan, T. Zhou, et al., Environ. Pollut. 265 (2020) 114864.
[12] J. Li, J. Zhang, S. Ren, et al., Sci. Total Environ. 877 (2023) 162947.
[13] R. Mao, M. Lang, X. Yu, et al., J. Hazard. Mater. 393 (2020) 122515.
[14] X. Qiu, S. Ma, J. Zhang, et al., Environ. Sci. Technol. 56 (2022) 10149–10160.
[15] L. Niu, Y. Li, Y. Li, et al., Water Res. 188 (2021) 116449.
[16] Y. Wang, M. Liu, C. Hu, et al., Chem. Eng. J. 433 (2022) 134048.
[17] Y. Wang, Y. Sun, R. Wang, et al., J. Hazard. Mater. 451 (2023) 130901.

[18] L. Roman, L. Lowenstine, L.M. Parsley, et al., Sci. Total Environ. 665 (2019) 660–667.
[19] K. Bhagat, A.C. Barrios, K. Rajwade, et al., Chemosphere 298 (2022) 134238.
[20] W. He, X. Wang, Y. Zhang, B. Zhu, H. Wu, J. Environ. Chem. Eng. 10 (2020) 109040.
[21] W. He, S. Zheng, X. Chen, D. Lu, Z. Zeng, J. Hazard. Mater. 438 (2022) 129568.
[22] D. Ma, J. Wu, P. Yang, M. Zhu, Environ. Sci. Technol. 54 (2020) 8801–8810.
[23] K. Matsunaga, T. Ohyama, K. Kuma, Y. Suzuki, Water Res. 29 (1995) 757–759.
[24] A. Lu, Y. Li, H. Ding, et al., Proc. Natl. Acad. Sci. U. S. A. 116 (2019) 9741–9746.
[25] S.A. Rich, P. Leroy, T. Dufour, et al., Surf. Interface Anal. 46 (2014) 164–174.
[26] J. Almond, P. Sugumaar, M.N. Wenzel, G. Hill, C. Wallis, De Gruyter 20 (2020) 369–381.
[27] M.C. Celina, E. Linde, E. Martinez, Polym. Degrad. Stab. 188 (2021) 109550.
[28] D. Briggs, N. Fairley, Surf. Interface Anal. 33 (2002) 283–290.
[29] P. Hu, M. Jiang, M. Chen, H.P. Li, Surf. Eng. 22 (2006) 327–330.
[30] P.N. Khanam, M.A.A. AlMaadeed, Adv. Manuf.: Polym. Comp. Sci. 1 (2015) 63–79.
[31] T. Sang, C.J. Wallis, G. Hill, C.J.P. Britovsek, Eur. Polym. J. 136 (2020) 109873.
[32] F. Gugumus, Makromol. Chem. Macromol. Symp. 27 (1989) 25–83.
[33] I. Velzeboer, C.J.A.F. Kwadijk, A.A. Koelmans, Environ. Sci. Technol. 48 (2014) 4869–4876.
[34] X. Guo, J. Wang, Mar. Pollut. Bull. 142 (2019) 1–14.
[35] Z. Wang, Z. Wu, S. Tang, Water Res. 43 (2009) 1533–1540.
[36] J. Hu, F.Y. Lim, J. Hu, Water Res. 232 (2023) 119628.
[37] Y.K. Lee, K.R. Murphy, J. Hur, Environ. Sci. Technol. 54 (2020) 11905–11914.
[38] M. Yuan, H. Xiang, Y. Tong, et al., Separations 10 (2023) 101–115.
[39] Y.K. Lee, S. Hong, J. Hur, Water Res. 190 (2021) 116775.
[40] Y.Y. Song, K.S. Park, H.K. Park, et al., J. Korean Phys. Soc. 52 (2008) 106–111.
[41] M. Li, S. Kuang, J. Dong, H. Ma, Y. Kang, J. Mol. Struct. 1275 (2023) 134624.
[42] H. Ouyang, C. Wu, X. Qiu, et al., Environ. Res. 217 (2023) 114874.
[43] H. Chi, P. Zhang, J. Xiong, et al., Appl. Surf. Sci. 608 (2023) 155116.
[44] L.S. Kau, D.J. Spira-Solomon, J.E. Penner-Hahn, K.O. Hodgson, E.I. Solomon, J. Am. Chem. Soc. 109 (1987) 6433–6442.
[45] J. Wang, J. Li, C. Jiang, et al., Appl. Catal. B 204 (2017) 147–155.
[46] W. Wei, C. Wang, X. Shi, et al., Water Res. 222 (2022) 118895.
[47] Y.K. Lee, J. Hur, Water Res. 187 (2020) 116426.
[48] P. Liu, L. Qian, H. Wang, et al., Environ. Sci. Technol. 53 (2019) 3579–3588.
[49] Y. Wang, Y. Sun, M. Gao, et al., J. Clean. Prod. 380 (2022) 134953.
[50] C. Wang, Z. Xian, X. Jin, et al., Water Res. 183 (2020) 116082.
[51] Y. Qiu, T. Zhang, P. Zhang, J. Hazard. Mater. 453 (2023) 131401.
[52] A. Halle, L. Ladirat, M. Martignac, et al., Environ. Pollut. 227 (2017) 167–174.